"Plasma Waves in Space & in the Laboratory." Vol. 2, Edinburgh Univ. Press, 1970.

Recent Rocket Measurements of AC Electric and Magnetic Fields in the Ionosphere

S.D.SHAWHAN and D.A.GURNETT

I. INTRODUCTION

On 21 September 1967 at 0738 UT the Javelin 8.45 sounding rocket was launched from Wallops Island, Virginia, to an altitude of 763 km. The scientific purpose of this experiment was to determine the amplitude and frequency spectra of naturally occurring electric and magnetic fields in the frequency range of 30 Hz to 10 kHz (VLF) and to ascertain the performance of different types of electric dipole antennas.

The payload instrumentation included six antenna systems and seven receivers for the simultaneous analysis of VLF magnetic and electric fields, an impedance measurement for determining the dipole antenna impedance, and a nosecone VLF transmitter for creating VLF signals from a known source in the ionosphere.

Figure 1 shows a photograph of the Javelin 8.45 payload with the antennas deployed. The two Storey-type (1965) electric dipole antennas were parallel to the x-axis and y-axis, respectively (E_x and E_y). The E_y antenna had solid conducting antenna elements 15.3 cm in diameter which were separated by 3.13 meters; the E_x antenna had non-conducting spherical grids. A third dipole antenna consisting of two spherical wire cages 6.02 cm in diameter and separated by 48.2 cm was supplied by Dr F.L.Scarf (TRW Systems, Inc.) for

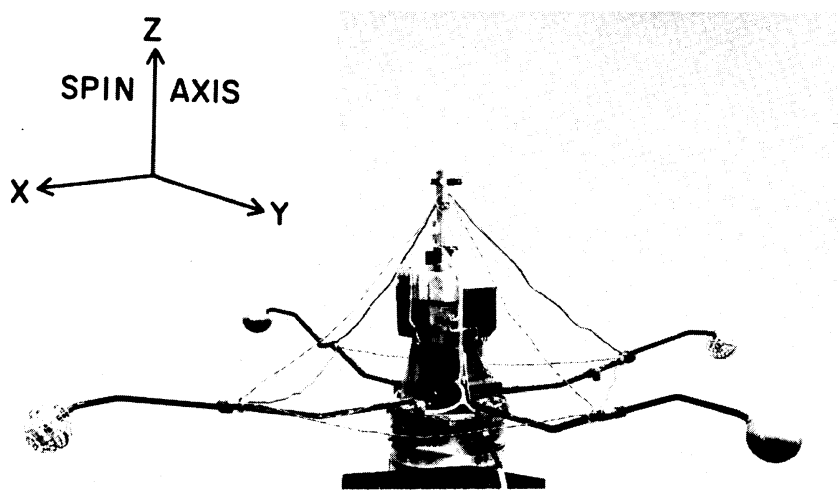

Fig. 1 Photograph of the Javelin 8.45 UI payload showing the antenna configuration.

comparison. It was located at the top of the payload and in Figure 1 is shown folded. The other three antennas were mutually orthogonal magnetic loops shown in Figure 1 running between the booms (called M_x, M_y and M_z). These loops consisted of three turns of No. 14 wire and were electrostatically shielded.

Each electric dipole antenna was connected to a wideband receiver by a differential preamplifier and each magnetic loop antenna by a transformer coupled preamplifier. The five wideband receivers consisted of two bandpass filters followed by compressor amplifiers which defined two independent frequency bands: a low frequency band of 30 Hz to 650 Hz and a high frequency band of 650 Hz to 10 kHz. These compressor amplifiers provided both wideband spectral information and r.m.s. amplitude information in that bandwidth. The E_x, E_y, M_x and M_y receivers were monitored continuously; the fifth wideband receiver was switched between the M_z and TRW antennas once every eight seconds. To obtain some amplitude information above 10 kHz a step frequency receiver was used with the E_y dipole antenna. This receiver had channels at 7.35, 10.5, 14.5, 22.0, 30.0, 40.0, 52.5 and 70.0 kHz with bandwidths of $\pm 7\frac{1}{2}\%$.

A more detailed discussion of the antenna systems and receivers as well as a description of the impedance measurement and nosecone VLF transmitter technique and results is given by Shawhan and Gurnett (1968).

This experiment, described briefly above, has the advantage that it can provide both spectral and amplitude information simultaneously for five of the six electromagnetic wave components. Therefore, the wave field geometry can be determined. Frequency-time spectrograms (0-10 kHz frequency scale and time in minutes after launch) from the E_x and M_y receivers are shown in Figure 2. Also amplitudes from the step frequency receiver are shown for six altitudes during the flight (log frequency scale 7.35 to 70.0 kHz and log voltage spectral density scale 10^{-13} to 10^{-16} volts^2 Hz^{-1}). Two predominant types of VLF noise are seen in Figure 2: a high frequency noiseband above 7 kHz and low frequency noise bursts below 1 kHz. The high frequency noiseband was observed in both the electric and magnetic receivers throughout the flight. It covered a band between 7 kHz and 30 kHz but both the upper and lower frequency limits decreased with increasing altitude. Table 1 gives a summary of the maximum and minimum field strengths for a magnetic, an electric and the TRW receivers (averaged over ±50 km). Both the magnetic and electric high band amplitudes (650 Hz-10 kHz) increased with altitude to peaks of 10 $m\gamma$ and 12 mV respectively. Results from the impedance measurement indicate that the potential drop through the E_x and E_y antenna sheaths was negligible. Therefore, the voltages in Table 1 for E_x can be interpreted as electric fields when divided by 3.13 meters. The observational data for this high frequency noise are summarized and discussed in the next section.

In Figure 2 noise, modulated at the payload precession rate, appears below 500 km in altitude (2 to 5 minutes and 12.5 to 15 minutes) and below 1 kHz in frequency. The noise amplitude as given for the low bands (30 Hz to 650 Hz) in Table 1 reached 20 mV over the apogee value of 0.3 mV on the electric antennas; the magnetic low

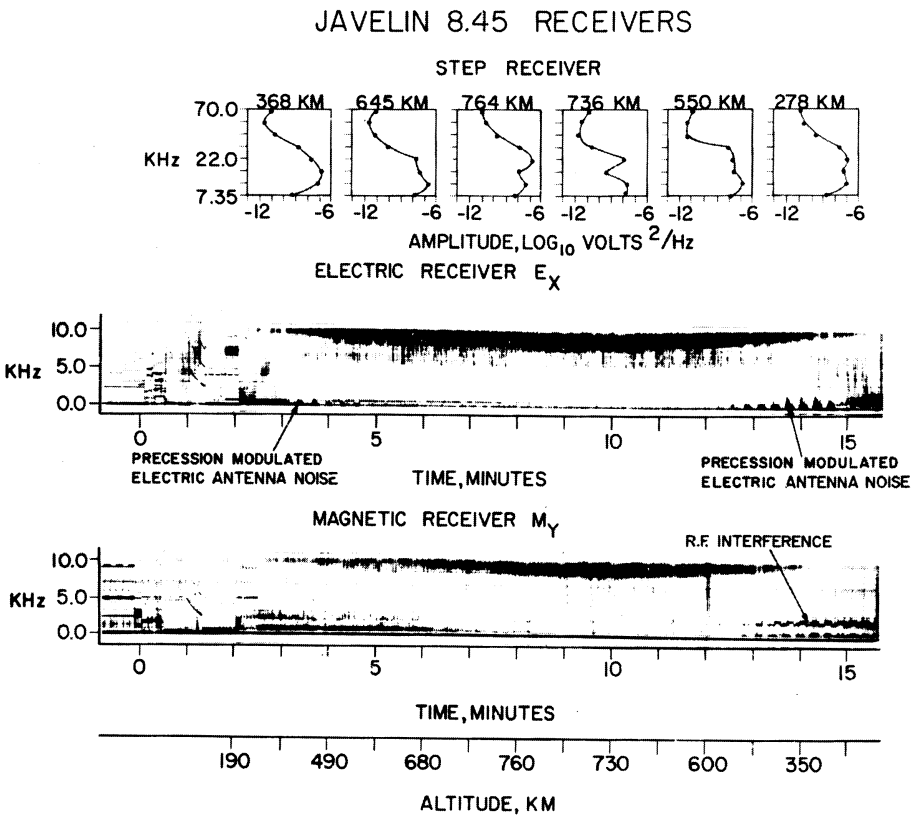

Fig. 2 Frequency spectra of the AC electric and magnetic fields observed during the flight showing the predominant high frequency electromagnetic noiseband above 7 kHz and the low frequency precession modulated electric antenna noise below 1 kHz and 500 km.

band however showed a nearly constant 10 $m\gamma$ amplitude throughout the flight. The observed characteristics of this low frequency noise are summarized and discussed in Section III.

Besides the predominant noiseband phenomena, hundreds of short fractional hop whistlers and 6 long hop whistlers were observed.

II. HIGH FREQUENCY ELECTROMAGNETIC NOISE BAND

The observational data about the high frequency noiseband observed between 7 and 30 kHz are presented in Figures 2, 3 and 4. Figure 2, as discussed in the previous section, shows the spectral characteristic of this noise band vs time for one electric, one magnetic and the step frequency receiver. In Figure 3 the lower cutoff frequency of this noiseband from the electric and magnetic receiver spectrograms is plotted against altitude and is compared to the lower hybrid resonance frequency assuming a realistic electron density model and a constant effective ion mass of 10.1 AMU. The amplitude variations of this noise band for two magnetic and two electric receivers are

Table 1. Summary of Wideband Receiver Signal Strengths*

Altitude km	Low Bands (30-650 Hz)						High Bands (0.65-10 KHz)					
	Magnetic Z milligammas		Electric X† millivolts		TRW† millivolts		Magnetic Y milligammas		Electric X† millivolts		TRW† millivolts	
	Max.	Min.	Max.	Min.	Max.	Min.	Max.	Min.	Max.	Min.	Max.	Min.
300 up	10.0	7.0	20.0	10.0	8.0	2.5	10.0	7.0	7.0	1.5	1.0	0.50
400 up	15.0	5.0	5.0	0.3	4.0	0.2	10.0	7.0	4.0	0.5	0.25	0.06
500 up	18.0	6.0	4.0	0.1	3.0	0.05	12.0	8.0	8.0	0.8	0.10	0.08
600 up	15.0	4.0	1.5	0.06	1.0	0.04	12.0	8.0	12.0	1.0	0.09	0.06
700 up	8.0	6.0	0.4	0.06	0.03	0.04	15.0	9.0	12.0	1.0	0.10	0.07
764 apogee	10.0	5.0	0.3	0.06	0.08	0.03	12.0	8.0	9.0	1.0	0.07	0.05
700 down	8.0	6.0	0.4	0.07	0.10	0.04	20.0	8.0	12.0	1.5	0.09	0.07
600 down	10.0	6.0	0.5	0.07	0.10	0.04	20.0	8.0	10.0	2.0	0.10	0.08
500 down	9.0	7.0	2.0	0.08	1.0	0.3	12.0	6.0	7.0	1.0	0.12	0.08
400 down	7.0	5.0	4.0	0.10	—		9.0	5.0	4.0	1.0	0.20	0.09
300 down	8.0	6.0	9.0	0.15	2.0	0.06	7.0	5.0	3.0	0.2	0.40	0.10
200 down	9.0	7.0	0.3	0.06	—		7.0	5.0	0.8	0.2	0.13	0.07
100 down	—		2.0	0.06	—		7.0	5.0	1.0	0.1	0.12	0.08

* Maximum and minimum value over approximately ±50 km.
† r.m.s. voltage difference between spheres.

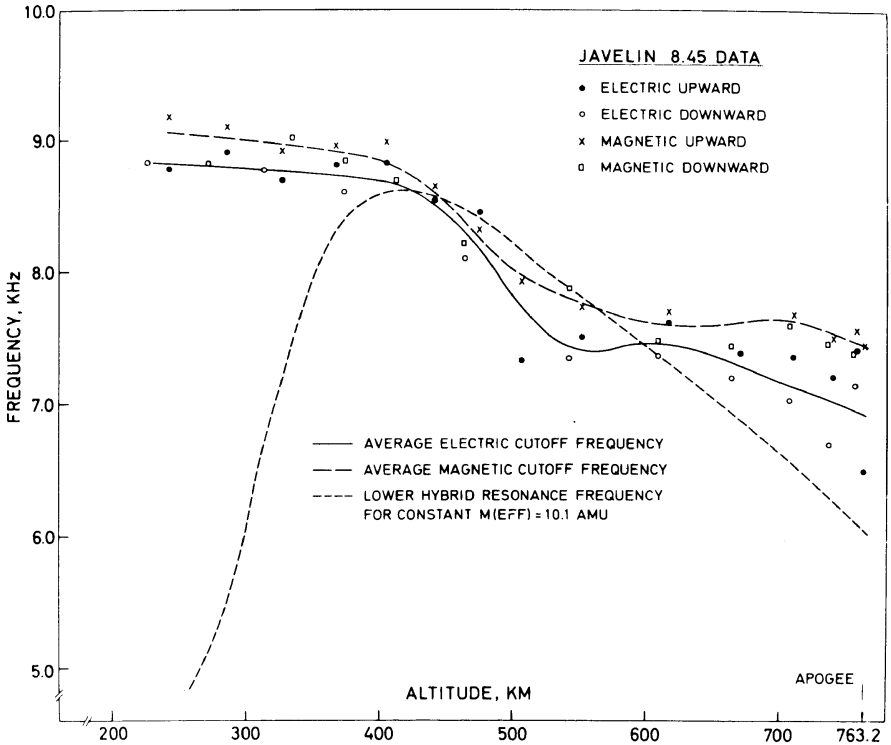

Fig. 3 Measurements of the magnetic and electric field cutoff frequency as altitude for the high frequency noiseband and a plot of the lower hybrid resonance frequency for a constant effective ion mass of 10.1 AMU.

compared to each other and to the geomagnetic field direction in Figure 4. The conclusions about the spectral characteristics, the noise amplitudes, and, the wave field geometry can be summarized as follows:

(1) Spectral Characteristics: From the electric receiver (E_x) and the step receiver results in Figure 2 it is seen that the noiseband was limited between about 7 kHz and 30 kHz but that both the upper and lower 'cutoff' frequencies decreased with altitude (30 to 22 kHz and 9.2 to 6.9 kHz). High resolution spectrograms indicate that the noise was a superposition of many noisebursts occurring on a time scale of tens of milliseconds. Several noise bursts are seen below the 'cutoff' frequency in only the electric field spectrogram. Figure 3 shows data points and smoothed curves for the lower cutoff frequency of this noise. Data are shown for the upward and downward legs for both the electric (●, ○ and solid line) and the magnetic (x, □ and dashed line) fields. The cutoff frequency decreased approximately as the geomagnetic field strength but the electric field noise has a consistently lower cutoff frequency. This cutoff frequency difference is 200 Hz at 200 km, a minimum of 100 Hz near 450 km and a maximum of 500 Hz at apogee.

(2) Noise Amplitudes: Because this noise was seen persistently on both the electric and the magnetic receivers and because the electric and magnetic field amplitudes had similar behaviour (see Table 1), it is concluded that this noise is electromagnetic. From the step receiver the peak electric field spectral density was measured to be 10^{-8} volts^{2}m^{-2}Hz^{-1} at 10 kHz and for a 2.5 kHz bandwidth the corresponding magnetic field spectral density was $4 \times 10^{-8}\gamma^2$Hz^{-1}.

(3) Wave Field Geometry: The simultaneous measurement of the electric and magnetic field components has provided information on the wave field geometry. Analysis of the field amplitudes has shown that the noiseband was strongly modulated at the precession rate (3.4 rpm, 27° half angle cone) and at the spin rate (11 rpm) of the payload. The most pronounced spin modulation occurred when the spin axis was very nearly perpendicular to the geomagnetic field ($\vec{B}_0$). Figure 4 compares the spin modulation of two magnetic and two electric receivers for the case that the spin axis was nearly perpendicular to $\vec{B}_0$ ($\theta_Z = 97°$ at 441 seconds). The magnetic field angles θ_X and θ_Y show that the X and Y axis alternately became aligned nearly parallel and nearly perpendicular to $\vec{B}_0$. For $\theta_X = 0°$ or 180° M_X and E_Y had maxima while M_Y and E_X had minima and conversely for $\theta_Y = 0°$ or 180°. Consequently the maxima in the magnetic field amplitude occurred when the axis of the loop was along B_0; the electric field maxima occurred when the antenna was perpendicular to $\vec{B}_0$. From Maxwell's equation $\nabla \cdot \vec{B} = 0$, the propagation vector $\vec{K}$ must be nearly perpendicular to $\vec{B}_0$ (most whistler waves would have $\vec{K}$ nearly parallel to $\vec{B}_0$).

Many features of this high frequency electromagnetic noiseband are similar to the lower hybrid resonance (LHR) noise observed with the Alouette 1 dipole receiver (Barrington et. al., 1964; Brice and Smith, 1964 and 1965; and McEwen and Barrington, 1967) and occasionally by the Injun 3 magnetic loop receiver (Gurnett, 1967). This LHR noise has a well-defined lower cutoff frequency and varies markedly with spatial changes between 4 and 15 kHz. The spectral characteristics and wave field geometry of the noise observed with Javelin 8.45 are consistent with the hypothesis that the lower cutoff frequency of this noise band is the local lower hybrid resonance frequency.

On Figure 3 is plotted a LHR frequency curve for a realistic electron density model and a constant ion effective mass of 10.1 AMU (for example 78% 0^+ and 22% He^+). The observed cutoff frequency curves fall within the same frequency range as the LHR frequency curve and have the same general decrease in frequency with altitude above 450 km (approximately proportional to $\vec{B}_0$). A decrease in the percentage of 0^+ above 450 km would cause the calculated LHR curve to decrease less rapidly with altitude. Below 400 km, however, the LHR frequency becomes proportional to the square root of the electron density and it must decrease very rapidly. Therefore, the observed cutoff frequency cannot be the LHR frequency below 400 km. The LHR frequency is an electrostatic resonance for propagation with wave normals ($\vec{K}$) perpendicular to $\vec{B}_0$. At the local LHR frequency E/B becomes very large which is consistent with the higher cutoff frequency for the magnetic field and the large electric fields observed. From the spin and precession modulation it was determined

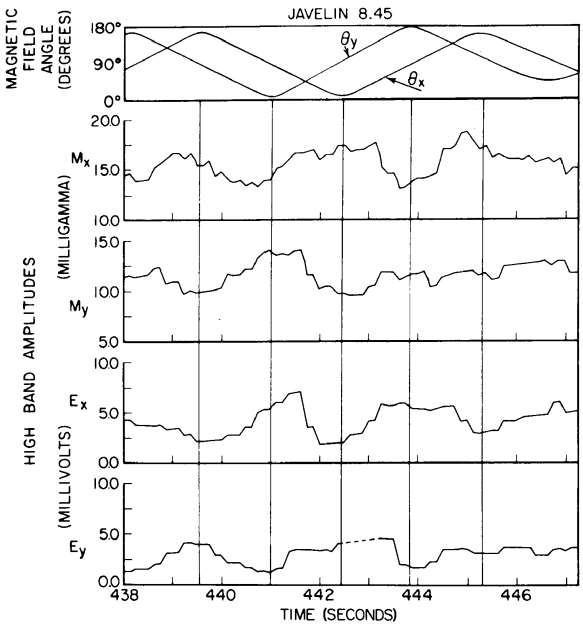

Fig. 4 Comparison of the magnetic and electric field spin modulation with the spin axis nearly perpendicular to the geomagnetic field ($\theta_X \simeq 90°$) for the high frequency noiseband.

that $\vec{K}$ was nearly perpendicular to $\vec{B}_0$. Waves propagating perpendicular to the geomagnetic field can be reflected at the altitude for which the wave frequency is just equal to the LHR frequency. For downcoming waves, higher and higher frequency components could be reflected with decreasing altitude giving a cutoff frequency at the LHR frequency that increases with decreasing altitude as observed. Frequency components below the maximum LHR frequency (8.62 kHz at 425 km in Figure 3) would then have been reflected at the higher altitudes and therefore would not be observable below the altitude of the maximum LHR frequency.

III. LOW FREQUENCY PRECESSION MODULATED NOISE

The observational data about the low frequency noise band observed below 1 kHz are shown in Figures 2, 5 and 6. Figure 2 shows the low frequency precession modulated electric antenna noise on the electric receiver spectrogram at altitudes less than 500 km on both the upward and the downward legs. In Figure 5 the frequency scale of the noise on the downward leg is expanded for the TRW, E_x and E_y receivers and the occurrence is compared to the spin and precession angles of the payload (θ_X, θ_Y and θ_Z) with respect to the geomagnetic field. The electric noise amplitude as seen on the three electric receivers is shown in Figure 6 plotted against θ_X, θ_Y and θ_Z for the upward leg of the flight. The conclusions about the spectral characteristics, the noise amplitude, and the wave field geometry can be summarized as follows:

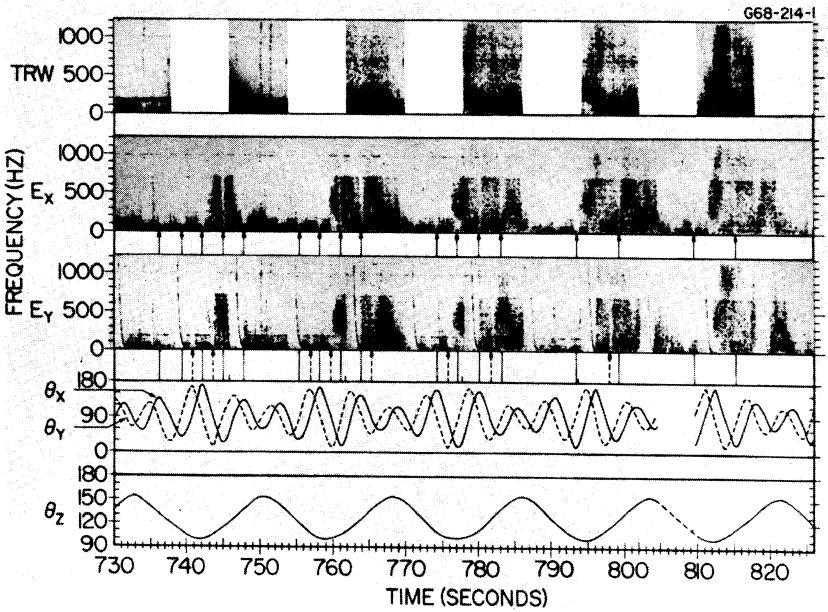

Fig. 5 Frequency spectra of the low frequency electric antenna noise near the end of the flight from all three electric antennas. Note the occurrence at the precession period.

(1) Spectral Characteristics: From Figure 5 it is seen that the period of the noise bursts was the same as the precession period of the payload. Spin period effects were much less pronounced. The precession modulation pattern consisted of a time interval for which the noise was absent followed by a rapid onset of the noise with the upper frequency limit rising very rapidly. On the spectrograms, the noise bursts were nearly symmetric and the maximum frequency decreased with increasing altitude (see Figure 2). Frequency-time structure on a time scale of tenths of seconds existed but it was usually different on all three antennas and was not related to the payload orientation.

(2) Noise Amplitude: The amplitudes for the receiver low bands (30 Hz to 650 Hz) are plotted in Figure 6 for the upward leg of the flight. This electric antenna noise showed variations in amplitude of nearly two orders of magnitude whereas the corresponding magnetic channels showed very little change throughout the flight (Table 1). Consequently this noise appears to be primarily electrostatic. For all three electric antennas, the maximum amplitude occurred at 225 km and was 20 mV for E_X and E_Y and 8 mV on TRW. The peak noise voltage spectral density was 6×10^{-7} volts^2/Hz.

(3) Wave Field Geometry: For the upgoing portion of the flight the maxima in the precession modulated amplitudes occurred when θ_Z was a maximum (spin axis 145° with respect to $\vec{B}_0$ in Figure 6) and the nulls occurred when the spin axis was perpendicular to $\vec{B}_0(\theta_Z = 90°)$. For the downgoing part of the flight, however, the noise amplitude was 90° out of phase with θ_Z. It was found that the noise

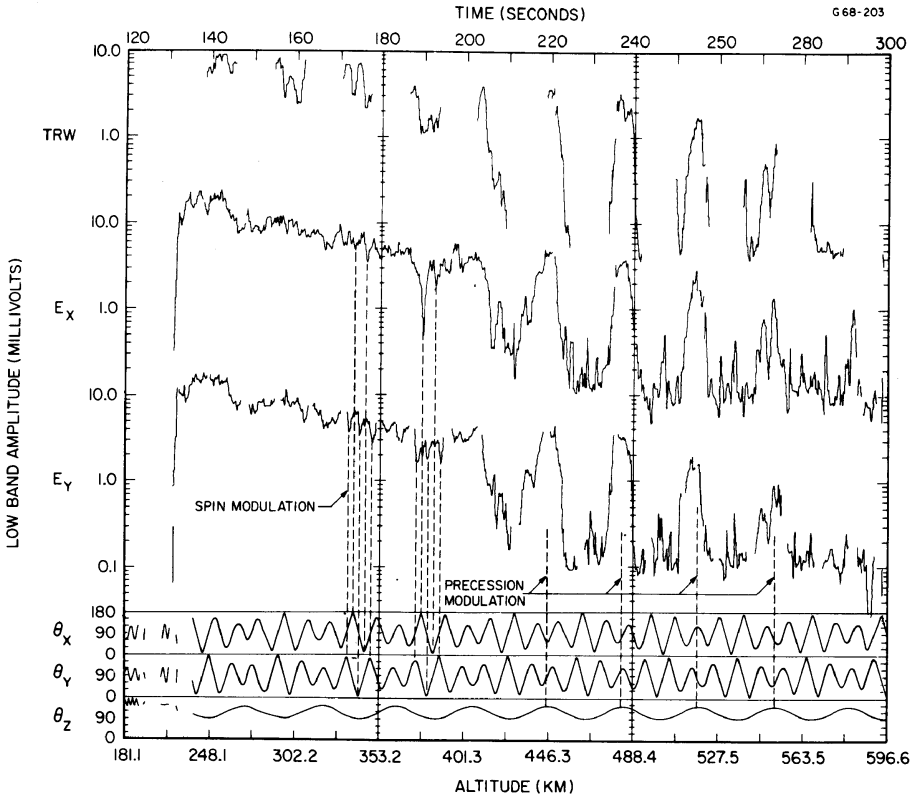

Fig. 6 Amplitude variation of the low frequency electric antenna noise at the beginning of the flight. The nosecone separated at 120 seconds (181 km altitude) and precession modulation does not begin until 190 seconds.

was in phase with the angle between the $\vec{Z}$-axis, and the component of the payload velocity perpendicular to $\vec{B}_0$, $\vec{V}_\perp$. When the angle between $\vec{V}_\perp$ and the Z-axis was a maximum, the noise amplitude and the frequency were also a maximum.

Similar precession modulated electric field noise has been reported by Iwai et. al., (1966) from the L-3-2 sounding rocket. This noise was observed below 337 km with a maximum intensity in the frequency range below 1. 5 kHz having strong precession modulation which was not consistent with a cosine law antenna pattern. Also Scarf (1965, 1966, 1967) has reported large AC electric fields in this frequency range at low altitudes with satellites 1964-45A and OV3-3.

Several possible sources for this large amplitude, electrostatic, low frequency noise have been considered: long wavelength electrostatic waves, short wavelength doppler shifted waves, antenna bias current fluctuations, and turbulent wake noise generated by the payload motion. It is concluded that this noise cannot be long wavelength electrostatic waves because the amplitude variations and the frequency spectrum envelope do not agree with a cosine law antenna pattern; because the amplitude is not proportional to the antenna

length when comparing the TRW and the longer dipole antennas; and because the signals on the TRW and the E_x and E_y antennas are not correlated. Since the noise signals are not correlated between the TRW antenna and the E_y or E_x antenna, it could be that the noise is doppler shifted waves with a wavelength of less than three meters. However, for the rocket velocity of 3 km/second and a wavelength of 1 meter, the resulting frequency would be 3 kHz which is inconsistent with the observed frequency spectra. Changes in the electric antenna bias current caused by the changing payload orientation could possibly produce the precession modulated noise (Dr Kellog, private communication). However, the maximum variation in the bias current was measured to be 10^{-8} amps which is significantly less than the incident ion current. Also, since the conducting (E_y) and the insulated (E_x) antennas agreed in noise amplitude, it appears unlikely that the noise could be antenna bias variations.

Because the fourth stage rocket bottle remained attached to the payload and was oriented in nearly the $\vec{V}_\perp$ direction, it is possible that the payload itself caused a turbulent wake in the plasma. A turbulent wake could cause large, short wavelength, electric fields which could appear with a non-cosine law variation, could be uncorrelated between the TRW and E_x or E_y antenna and not proportional to the antenna length, and which could have a frequency spectrum below 1 kHz. Also the predominant precession modulation, the correlation with the angle between the spin axis and $\vec{V}_\perp$, and the lack of large spin modulation is more understandable with the wake hypothesis. During the time period of one minute after nosecone separation the electric field noise amplitude was four times the amplitude of the same altitude range for the downward leg of the flight and no precession modulation was observed. Possibly the nosecone created a large wake as it separated from the payload which caused this large amplitude electrostatic noise. This possible nosecone effect provides further evidence for the hypothesis that this noise is caused by the motion of the payload through the ionosphere and not by naturally occurring noise phenomena.

REFERENCES

Barrington, R. E., J. S. Belrose, and D. A. Keeley, 'Very Low Frequency Noise Bands Observed by the Alouette 1 Satellite,' J. Geophys. Res. 68, 6539-6541 (1963).

Brice, N. M., and R. L. Smith, 'A Very Low Frequency Plasma Resonance,' Nature 203, 926 (1964).

Brice, N. M., and R. L. Smith, 'Lower Hybrid Resonance Emissions,' J. Geophys. Res. 70, 71-80 (1965).

Gurnett, D. A., 'Satellite Observations of VLF Emissions and Their Association with Energetic Particles,' Department of Physics and Astronomy, University of Iowa, Iowa City, Iowa, Res. Rept. 67-53 (1967).

Iwai, A., J. Outsu, and Y. Tanaka, 'The Observation of ELF-VLF Radio Noise with Sounding Rockets L-3-2, K-9M-6,' Proceedings of the Research Institute of Atmospherics, Nagoya University, Vol. 13, January 1966.

McEwen, D. J., and R. E. Barrington, 'Some Characteristics of the Lower Hybrid Resonance Noise Bands Observed by the Alouette 1 Satellite,' Canadian J. of Physics, Vol. 45, 13-19 (1967).

Scarf, F. L., G. M. Crook, and R. W. Fredricks, 'Preliminary Report on Detection of Electrostatic Ion Waves in the Magnetosphere,' J. Geophys. Res. 70, (13), 3045-3060 (1965).

Scarf, F. L., G. M. Crook, and R. W. Fredricks, 'Survey of VLF Electric fields in the Magnetosphere with the Polar Orbiting Spacecraft,' 1964-45A, Radio Science, Vol. 1, (New Series), No. 8, August 1966.

Scarf, F. L., R. W. Fredricks, and G. M. Crook, 'Detection of Electromagnetic and Electrostatic Waves on OV3-3,' TRW Systems Rept. 09485-6001-Rooo, Redondo Beach, California (1967).

Shawhan, S. D. and D. A. Gurnett, 'VLF Electric and Magnetic Fields Observed with the Javelin 8.45 Sounding Rocket', Dept. Physics and Astron., Univ of Iowa Research Report, February 1968, also submitted to J. Geophys. Res.

Storey, L. R. O., 'Antenne Electrique Dipole Pour Reception TBF Dans L'Ionosphere,' L'onde Electrique, t. XLV, No. 465, December 1965.